Draft version April 19, 2012
Preprint typeset using LaTeX style emulateapj v. 03/07/07

IN THE CRUCIBLE: MASSIVE COMPACT GALAXIES WITH HIGH-VELOCITY OUTFLOWS AND EDDINGTON-LIMITED STAR FORMATION

Aleksandar M. Diamond-Stanic[1,2], John Moustakas[1], Christy A. Tremonti[3], Alison L. Coil[1], Ryan C. Hickox[4], Aday Robaina[5], Gregory H. Rudnick[6], & Paul Sell[3]

Draft version April 19, 2012

ABSTRACT

We present the discovery of compact, obscured star formation in galaxies that exhibit $\gtrsim 1000$ km s^{-1} outflows. Using optical morphologies from the Hubble Space Telescope and infrared photometry from the Wide-field Infrared Survey Explorer, we estimate star formation rate (SFR) surface densities that approach $\Sigma_{\rm SFR} \approx 5000$ M$_\odot$ yr^{-1} kpc^{-2}, which is comparable to the Eddington limit from radiation pressure on dust grains. We argue that feedback associated with a compact starburst in the form of radiation pressure from massive stars and ram pressure from supernovae and stellar winds is sufficient to produce the high-velocity outflows we observe, without the need to invoke feedback from an active galactic nucleus.

Subject headings: galaxies: evolution — galaxies: kinematics and dynamics — galaxies: ISM — galaxies: starburst

1. INTRODUCTION

The central regions of elliptical galaxies are thought to form in compact starbursts (e.g., Kormendy et al. 2009; Hopkins et al. 2009). Feedback associated with such starbursts can produce outflows driven by thermal energy from supernova explosions (e.g., Chevalier & Clegg 1985), stellar winds (e.g., Leitherer et al. 1992), and momentum input from both supernova ram pressure and radiation pressure on dust grains (e.g., Murray et al. 2005). It has been argued that such feedback imposes a limit on the maximum star-formation rate surface density ($\Sigma_{\rm SFR}$) for starbursts (e.g., Lehnert & Heckman 1996; Meurer et al. 1997; Murray et al. 2005; Thompson et al. 2005) and the maximum stellar surface density for elliptical galaxies and star clusters (e.g., Hopkins et al. 2010).

Galactic winds are ubiquitous in star-forming galaxies at all redshifts and generally exhibit outflow velocities in the 100–500 km s^{-1} range (e.g., Heckman et al. 2000; Shapley et al. 2003; Martin 2005; Rupke et al. 2005; Weiner et al. 2009; Rubin et al. 2010; Steidel et al. 2010). Thus, the discovery of $|v| > 1000$ km s^{-1} outflows in a sample of massive ($M_* \approx 10^{11}$ M$_\odot$) post-starburst galaxies at $z \sim 0.6$ by Tremonti et al. (2007) suggested that a more energetic source, such as feedback from an accreting supermassive black hole (e.g., Silk & Rees 1998; Di Matteo et al. 2005; Debuhr et al. 2012), could have been responsible for launching the winds (see Fabian 2012, for a recent review).

However, it also plausible that feedback from a compact starburst could expel gas with such large velocities. Indeed, there is evidence for a positive correlation between outflow velocity and starburst luminosity (e.g., Martin 2005; Rupke et al. 2005; Tremonti et al. 2007), albeit with significant scatter. Furthermore, Heckman et al. (2011) recently found outflows with maximum velocities reaching -1500 km s^{-1} in a sample of local starbursts with compact nuclei, and argued that such velocities could be explained by feedback from massive stars.

In this Letter, we present results for a sample of massive galaxies at $z \sim 0.6$ that exhibit $|v| \gtrsim 1000$ km s^{-1} outflows, expanding on the sample from Tremonti et al. (2007). We seek to test whether the energetic outflows in these galaxies could have been driven by feedback from starbursts with very large star-formation rate (SFR) surface densities ($\Sigma_{\rm SFR}$). Our analysis combines galaxy sizes obtained with the Hubble Space Telescope (HST) with star-formation rates and stellar masses estimated from WISE, Spitzer, SDSS, and GALEX photometry.

2. ANALYSIS

2.1. *Morphologies and Sizes*

Our sample derives from 29 galaxies targeted for HST/WFC3 imaging in programs 12019 and 12272 (PI: C. Tremonti). Using the F814W filter on the UVIS channel, which has 0.04″ pixels and FWHM = 0.074″, we obtained 4×10 min exposures in a single orbit for each galaxy. The dithered images were processed with MultiDrizzle[7] to produce science mosaics with 0.02″ pixels. For each galaxy, we use GALFIT (Peng et al. 2002, 2010) to model the two-dimensional surface brightness profile with a single Sersic component, using stars in the images to construct the model point-spread function (PSF). The Sersic index (n) and effective radius (r_e) are free parameters in the model. In cases where the best-fit model returns $n > 4$, we also fit an $n = 4$ de Vaucouleurs model (de Vaucouleurs 1948), yielding a larger r_e value (due to the covariance between n and r_e), and we use these these larger effective radii in our analysis.

For this paper, we are most interested in the galaxies with the largest $\Sigma_{\rm SFR}$ values, which also have the small-

[1] Center for Astrophysics and Space Sciences, University of California, San Diego, La Jolla, CA 92093, USA
[2] Center for Galaxy Evolution Fellow
[3] Department of Astronomy, University of Wisconsin-Madison, Madison, WI 53706, USA
[4] Department of Physics and Astronomy, Dartmouth College, Hanover, NH 03755, USA
[5] Institut de Ciéncies del Cosmos, University of Barcelona, 08028 Barcelona, Spain
[6] Department of Physics and Astronomy, University of Kansas, Lawrence, KS 66045, USA

[7] http://stsdas.stsci.edu/multidrizzle/

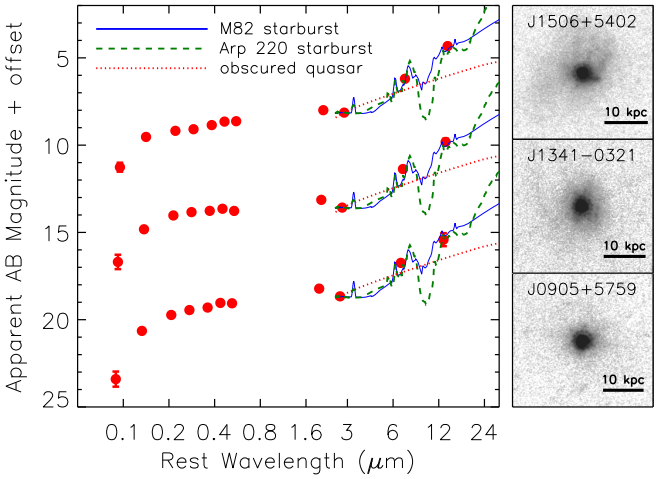

FIG. 1.— Left: Observed UV–IR SEDs ($\lambda_{\rm rest}$ = 0.1–15 μm) for three galaxies with large SFR surface densities ($\Sigma_{\rm SFR}$ > 3000 $M_\odot$ yr^{-1} kpc^{-2}). We show stellar population fits to the $\lambda_{\rm rest}$ = 0.1–3 μm emission (black solid line) and three templates for dust emission (M82 starburst, Arp 220 starburst, and obscured quasar; Polletta et al. 2007). The starburst templates provide reasonable fits to the $\lambda_{\rm obs}$ = 12 and 22 μm WISE photometry, while the quasar template does not. Right: HST/WFC3 F814W images (probing $\lambda_{\rm rest} \approx$ 5000 Å) showing that these galaxies are dominated by a compact nucleus.

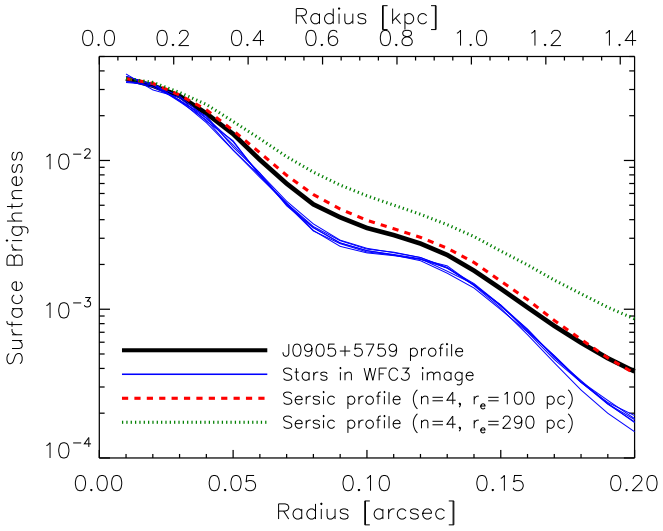

FIG. 2.— One-dimensional surface brightness profile for J0905+5759, which has the smallest effective radius in the sample. The observed profile is shown as the solid black line, and the profiles of six stars in the same image are shown in blue. The best-fit de Vaucouleurs profile with r_e = 100 pc is shown as a dashed red line, and for comparison a broader profile with $r_e = 0.04'' = 290$ pc is shown as the dotted green line. This galaxy is quite compact, but is more extended than a point source.

est effective radii. We show the HST images for three high-$\Sigma_{\rm SFR}$ galaxies in Figure 1. In all three cases, the single-component model GALFIT accounts for > 85% of the total flux. The residuals show diffuse emission that is consistent with these systems being late-stage galaxy mergers after final coalescence, although we defer a detailed comparison of the observed morphologies with expectations from merger simulations to future work.

For the most compact galaxy (J0905+5759, r_e = 0.013″ or 100 pc), we also show the observed one-dimensional surface brightness profile in the bottom-right panel of Figure 2.1. We compare to the profiles of six stars in the same image, the best-fit de Vaucouleurs model, and a de Vaucouleurs model with a larger effective radius (r_e = 0.04″, the native WFC3/UVIS pixel size, which corresponds to a physical scale of 290 pc). This comparison illustrates that this galaxy, while only marginally resolved with an effective radius that is ∼ 20% of the image FWHM, is clearly more extended than a point source.

For such a compact source, there is significant uncertainty in our r_e measurement given uncertainties in the model PSF. To quantify this uncertainty, we used TinyTim to generate a model PSF that is artificially narrower than the stars in the image (convolving the output of tiny2 with a FWHM = 0.04″ Gaussian, whereas the image FWHM is 0.074″) and found that this increased the effective radius in the GALFIT model by a factor of two. We also fit a two-component PSF+Sersic model, but found that the Sersic component dominates the fit, yielding a similar effective radius. Furthermore, the spectrum of the galaxy shows no evidence for an AGN contribution to the I-band continuum (see Figure 3), so there is no clear motivation for including an unresolved, point-source component in the model. We conclude that this galaxy is quite compact and that our r_e estimate of 100 pc, while uncertain, is likely accurate within a factor of two.

2.2. *Star Formation Rates and Stellar Masses*

We gathered photometry from the All-Sky Release of the Wide-field Infrared Survey Explorer (WISE, Wright et al. 2010), the Seventh Data Release of the Sloan Digital Sky Survey (SDSS, Abazajian et al. 2009), and General Release 6 from the Galaxy Evolution Explorer (GALEX, Martin et al. 2005). We also obtained 5×30 sec dithered exposures at 3.6 μm and 4.5 μm for all sources with the Infrared Array Camera (Fazio et al. 2004) on the Spitzer Space Telescope (Werner et al. 2004) as part of General Observer program 60145 (PI: C. Tremonti). We used the post–basic calibrated data to perform aperture photometry on all sources, and we also used the APEX[8] point-source extraction software for photometry of sources in crowded fields. All the photometry was corrected for Galactic extinction based on the Schlegel et al. (1998) dust maps. We show spectral energy distributions (SEDs) for the three high-$\Sigma_{\rm SFR}$ galaxies in Figure 1.

We estimate IR-based star-formation rates for the 25/29 galaxies with WISE 12 or 22 μm detections by fitting Chary & Elbaz (2001) templates to their 12 and 22 μm fluxes. For the 14/29 galaxies with 22 μm detections, this yields SFRs that agree with those obtained from the Rujopakarn et al. (2012) method based on 24 μm luminosity with a scatter of 0.05 dex. We note that several authors have shown that the shape of the IR SED for star-forming galaxies depends on the surface density of star formation (e.g., Rujopakarn et al. 2011; Elbaz et al. 2011), with more compact starbursts having larger total-IR (8–1000 μm) to mid-IR (8–24 μm) ratios.

[8] http://irsa.ipac.caltech.edu/data/SPITZER/docs/dataanalysistools/tools/n

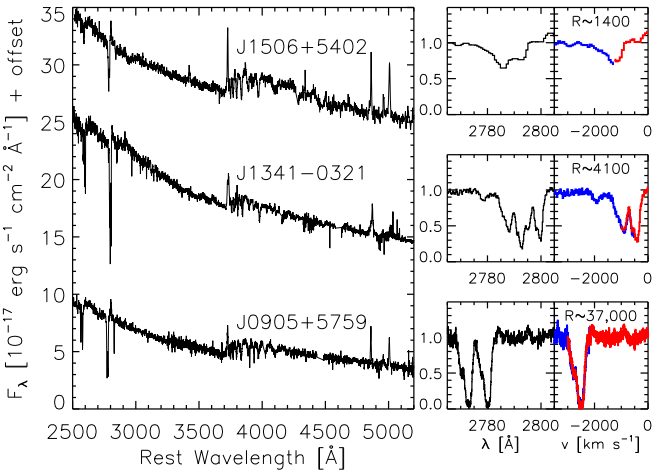

FIG. 3.— Spectra covering $\lambda_{\rm rest}$ = 2500–5200 Å for the three galaxies shown in Figure 1. These spectra are dominated by light from the young stellar population and exhibit [O II] λ3727, Hβ λ4861, and [O III] λ5007 emission lines. The panels on the right highlight the Mg II $\lambda\lambda$2796, 2803 spectral region in both wavelength and velocity space to illustrate the outflow kinematics. The spectrum in the bottom panel has sufficient spectral resolution (FWHM $\approx$ 8 km s^{-1}) to resolve the intrinsic shape of the absorption-line profile, revealing that the gas near the centroid velocity ($v = -2470$ km s^{-1}) covers the entire galaxy.

The extreme $\Sigma_{\rm SFR}$ values of our sample imply large total-IR to mid-IR ratios, characteristic of the most luminous galaxies in the local universe (e.g., Chary & Elbaz 2001; Dale & Helou 2002; Rieke et al. 2009). If we used the most luminous local templates for the 8/29 sources with SFRs in the ULIRG regime (SFR$_{\rm IR}$ > 200 M$_\odot$ yr^{-1}), we would obtain SFRs that are larger by 0.5 dex than the values we adopt for this paper.

We also estimate star-formation rates and stellar masses based on stellar population fits to the $\lambda_{\rm rest}$ = 0.1–3 μm SEDs using the method of Moustakas et al. (2011). For galaxies with SFR$_{\rm IR}$ > 50 M$_\odot$ yr^{-1}, there is agreement between these UV-based SFR estimates and SFR$_{\rm IR}$ with a scatter of 0.32 dex. For an SMC dust law, we find a median attenuation of $A_V = 0.4$ mag.

2.3. *Outflow Kinematics and Covering Factors*

We present $\lambda_{\rm rest}$ = 2500–5200 Å spectroscopy for three high-$\Sigma_{\rm SFR}$ sources in Figure 3 based on data from MMT/Blue Channel and SDSS (J1506+5402), Magellan/MAGE (J1341-0321), and Keck/LRIS and Keck/HIRES (J0905+5759). The spectra are dominated by light from the young (t < 50 Myr) stellar population. We highlight the Mg II $\lambda\lambda$2796, 2803 absorption lines, which are used used to measure outflow velocities. At low spectral resolution (e.g., the top right panel of Figure 3) it is not possible to determine the intrinsic shape of the absorption line profile and therefore the covering factor of the outflowing gas. However, the Keck/HIRES spectrum of J0905+5759 (FWHM $\approx$ 8 km s^{-1}) reveals that the gas covers the entire continuum source near the velocity centroid ($v = -2470$ km s^{-1}) indicating a galaxy-wide outflow.

3. DISCUSSION

The compact sizes ($r_e \approx 100$ pc) and large star formation rates (SFR $\approx$ 300 M$_\odot$) for the galaxies described above implies extremely large star-formation rate surface densities ($\Sigma_{\rm SFR} \approx 5000$ M$_\odot$ yr^{-1} kpc^{-2}). To place these galaxies in context, we plot their $\Sigma_{\rm SFR}$ values as a function of stellar mass in Figure 4. We include comparison samples of $\sim 10^5$ star-forming galaxies at $0.5 < z < 1.5$ from Wuyts et al. (2011) and a few dozen gas-rich mergers at $z < 0.3$ including 32 ULIRGs from Veilleux et al. (2006), five Lyman break analogs with dominant central objects from Overzier et al. (2009), and the local compact starburst Arp 220 (Scoville et al. 1997; Kennicutt 1998; Rodríguez Zaurín et al. 2008). We also mark the empirical threshold for launching winds ($\Sigma_{\rm SFR} \approx$ 0.1 M$_\odot$ yr^{-1} kpc^{-2}, Heckman 2002), the 90th percentile limit for the surface brightness of starbursts measured using UV, Hα, far-IR, and radio continuum emission ($\Sigma_{\rm SFR} \approx$ 45 M$_\odot$ yr^{-1} kpc^{-2} Meurer et al. 1997), and the theoretical limit for a starburst limited by feedback from radiation pressure ($\Sigma_{\rm SFR} \approx$ 2000 M$_\odot$ yr^{-1} kpc^{-2}, Murray et al. 2005; Thompson et al. 2005; Hopkins et al. 2010). The most luminous, compact starbursts in our sample exhibit SFR surface densities that reach the Eddington limit, suggesting that their growth is being regulated by momentum input from massive stars.

3.1. *Constraints on Ongoing AGN Activity*

While the SEDs (Figure 1) and optical spectra (Figure 3) for our sample indicate that their bolometric output is dominated by star formation, it is worthwhile to consider the level of ongoing AGN activity and its effect on our measurements. Among the high-$\Sigma_{\rm SFR}$ galaxies, the strongest case for detectable AGN emission can be made for J1506+5402, which has the most luminous [O III] λ5007 line among the 29 galaxies observed by HST. This source also has a weak [Ne V] λ3426 emission line, which is associated with AGN activity (e.g., Abel & Satyapal 2008; Gilli et al. 2010). It was observed with the Chandra X-ray Observatory (proposal ID 11700896, PI: C. Tremonti) and had four detected counts, corresponding to a 0.5–8.0 keV X-ray luminosity of $10^{42.7}$ erg s^{-1} (see P. Sell et al., in preparation for more details on the 12/29 galaxies with Chandra observations). Using the relationship between 2–10 keV X-ray and 12.3 μm mid-IR luminosity for AGNs from Gandhi et al. (2009), one would expect a source with $L_{\rm X} \approx 5\times10^{42}$ erg s^{-1} to have $L_{\rm MIR} \approx 7\times10^{42}$ erg s^{-1}, which is 400$\times$ smaller than observed luminosity for J1506+5402 ($L_{\rm MIR} \approx 3\times10^{45}$ erg s^{-1}). Based on its [O III] luminosity ($10^{42.1}$ erg s^{-1}, a significant fraction of which could be attributed to star formation) and the calibration for type 1 AGNs from Heckman et al. (2005), one would expect an intrinsic 2–10 keV luminosity of $L_{\rm X} \approx 5\times10^{43}$ erg s^{-1}, suggesting absorption by a factor of $\sim$ 10 in the X-rays. However, even if the X-ray attenuation were a factor of 100, which is the typical value for local Compton-thick AGNs (Diamond-Stanic et al. 2009), the expected mid-IR AGN contribution would only be relevant at the $\lesssim$30% level. Thus, similar to local ULIRGs (e.g., Farrah et al. 2007), the bolometric output of the galaxies in our sample is dominated by star formation, and we conclude that our results regarding large $\Sigma_{\rm SFR}$ values are not affected by AGN contamination.

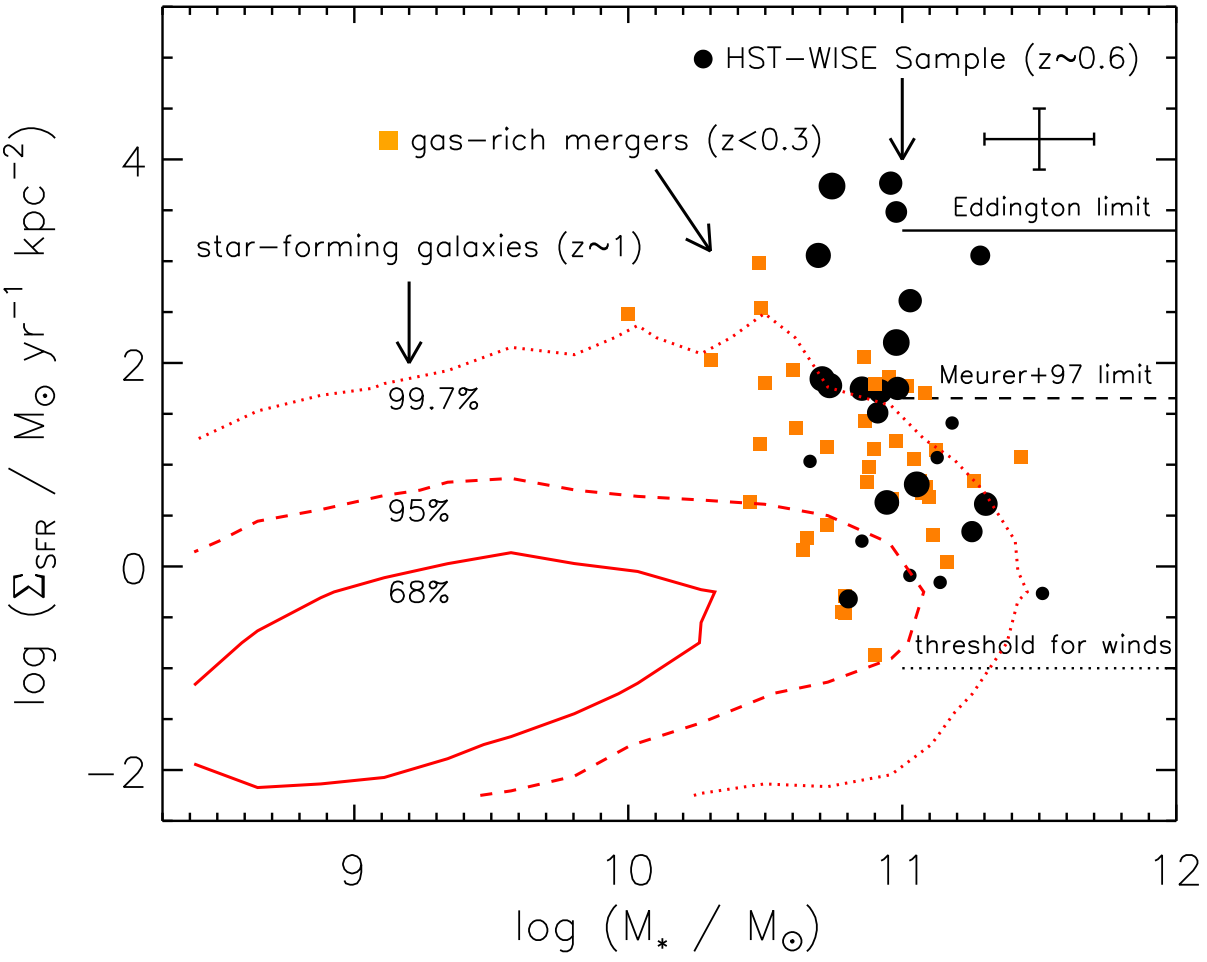

FIG. 4.— SFR surface densities and stellar masses for the HST–WISE sample described in this paper (black circles, with symbol size proportional to outflow velocity), along with samples of gas-rich mergers (orange squares) and star-forming galaxies (shown with 68%, 95%, and 99.7% contours). We mark the empirical threshold for launching winds (dotted line, $\Sigma_{\rm SFR} \approx 0.1$ M$_\odot$ yr^{-1} kpc^{-2}; Heckman 2002), the 90th-percentile starburst intensity limit from Meurer et al. (1997) (dashed line, $\Sigma_{\rm SFR} \approx 45$ M$_\odot$ yr^{-1} kpc^{-2}), and the Eddington limit from radiation pressure on dust grains (solid line, $\Sigma_{\rm SFR} \approx 2000$ M$_\odot$ yr^{-1} kpc^{-2}; Murray et al. 2005; Thompson et al. 2005; Hopkins et al. 2010). Our HST–WISE sample overlaps with the region characterized by gas-rich mergers, and extends to very large SFR surface densities near the Eddington limit, suggesting growth that is limited by momentum injection from massive stars.

3.2. *The Outflow Launching Mechanism*

It is worth considering whether the high-velocity outflows we observe were produced by the compact starburst. Murray et al. (2011) argued that massive star clusters with large gas surface densities are the ideal launching point for galactic-scale outflows driven by radiation pressure, and that the outflow velocity should scale with escape velocity of the most massive star clusters in a galaxy. The $\gtrsim 1000$ km s^{-1} outflow velocities we observe correspond approximately to the escape velocities for a compact stellar population with the sizes and masses that we've measured.

$$v_{esc} = \sqrt{2GM_*/r}$$
$$= 2100 \left(\frac{M_*}{10^{11} M_\odot}\right)^{1/2} \left(\frac{r}{200 \text{ pc}}\right)^{-1/2} \text{km s}^{-1} \quad (1)$$

This argument, combined with the fact that we observe galaxies with significant dust-obscured star formation and $\Sigma_{\rm SFR}$ values near the Eddington limit, indicates that momentum input from massive stars in the form of radiation pressure is a viable mechanism for launching these outflows.

In addition to radiation pressure, we also expect significant momentum flux from stellar winds and supernovae. For example, a starburst with SFR ≈ 200 M$_\odot$ yr^{-1} would be associated with radiation pressure $L_{bol}/c \approx 2 \times 10^{35}$ dyne and ram pressure $\dot{p} \approx 5$–10×10^{35} dyne from stellar winds and supernovae (e.g., Leitherer et al. 1992; Heckman et al. 1993; Leitherer et al. 1999; Veilleux et al. 2005). Furthermore, Heckman et al. (2011) noted that such a large momentum injection ($\dot{p} \approx 10^{35}$ dyne) from a small initial radius $r_0 \approx 100$ pc could accelerate a cloud with column density $N_H \approx 10^{21}$ cm^{-2} to a terminal velocity $v_\infty \approx 1800$ km s^{-1}. Thus, the energetics of compact starbursts are sufficient to produce the high-velocity outflows we observe, and it is plausible that both radiation pressure on dust grains and supernova ram pressure

contribute to driving the winds.

3.3. *Placing These Galaxies in Context*

The high-$\Sigma_{\rm SFR}$ galaxies in our sample constitute a rare population (see Figure 4), suggesting that they represent an unusual or short-lived phase. Mergers of gas-rich galaxies are a viable mechanism for producing compact starbursts (e.g., Mihos+94), but such gas-rich major mergers are rare at $z \sim 0.6$ due to the decline in both the merger rate and the gas fraction of galaxies since $z \sim 1$. The high-$\Sigma_{\rm SFR}$ galaxies are also in a particular phase where there is strong feedback but star formation has not been quenched. The length of this phase may be set by the gas consumption timescale or the timescale for feedback to suppress subsequent star formation. Based on the Kennicutt–Schmidt (K-S) relation (Kennicutt 1998), a galaxy with $r_e \approx 100$ pc, SFR ≈ 300 M$_\odot$, and $\Sigma_{\rm SFR} = 5000$ M$_\odot$ yr^{-1} kpc^{-2} (assuming half of the star formation occurs within the effective radius) would have a gas surface density of $\Sigma_{gas} \sim 2 \times 10^5$ M$_\odot$ pc^{-2}, corresponding to $M_{gas} \sim 5 \times 10^9$ M$_\odot$ inside 100 pc, which would be consumed on a timescale ~ 30 Myr. Such estimates could be tested with observations of molecular gas masses and kinematics for these extreme galaxies.

The vertical sequence among the galaxies in our sample in Figure 4 could be related to an evolutionary sequence, with smaller $\Sigma_{\rm SFR}$ galaxies being further along in their evolution towards a post-starburst phase. However, it is interesting to note that all 12/29 galaxies above the Meurer et al. (1997) limit ($\Sigma_{\rm SFR} \approx 45$ M$_\odot$ yr^{-1} kpc^{-2}) exhibit outflows (with median centroid velocity $v = -1500$ km s^{-1}), while all 7/29 galaxies without detected outflows have $\Sigma_{\rm SFR} < 30$ M$_\odot$ yr^{-1} kpc^{-2}. If a compact starburst is a requirement for the production of high-velocity outflows, as suggested by previous the discussion in Section 3.2, it may be that the non-outflow sources have not gone through such a phase (see A. Robaina, et al., in preparation for a discussion of the relationship between outflow velocity, galaxy morphology, and stellar population age).

Finally, it is worthwhile to consider the implications of these galaxies for models of massive galaxy formation. While simulaitons of major galaxy mergers with large gas fractions ($f_{gas} \sim 50\%$) can produce M$_* \sim 10^{11}$ M$_\odot$ remnants with effective radii $r_e \sim 1$ kpc (e.g., Wuyts et al. 2010), similar to the observed sizes of compact quiescent galaxies at $z \sim 2$ (e.g., van Dokkum et al. 2008), our sample includes galaxies of similar mass that are smaller by almost an order of magnitude. If these systems do evolve into quiescent elliptical galaxies, it would be quite challenging for them to grow in size from $r_e \sim 0.1$ kpc to $r_e \sim 5$ kpc to reach the local size–mass relation in the $t \sim 6$ Gyr since $z = 0.6$. In this context, it is relevant point to note that the half-light radius (ignoring dust attenuation) at rest-frame V band (where our HST observations prbe) can be a factor of 5–10 smaller than the half-mass radius for a system near the peak of the starburst (Wuyts et al. 2010). It would be worthwhile to test for such size discrepancies and to pronbe the radial dependence of the mass-to-light ratio by measuring sizes at rest-frame near-IR wavelengths.

4. CONCLUSIONS

Their descendants could perhaps be the local galaxies that are significant outliers from the size–mass relation.

Models that produce ellipticals have to invoke AGN feedback to quench star formation.

Few galaxies exhibit such high-velocity outflows because few galaxies have such extreme SFR surface densities.

Theoretical arguments about ram v. radiation pressure. Point that we are observing 10^4 K gas.

Mention high-$\Sigma_{\rm SFR}$ galaxies at high z.

High-velocity outflows do not imply AGN feedback.

We acknowledge useful discussions with and assistance from several people. AMD acknowledges support from the Southern California Center for Galaxy Evolution, a multi-campus research program funded by the University of California Office of Research.

REFERENCES

Abazajian, K. N., Adelman-McCarthy, J. K., Agüeros, M. A., et al. 2009, ApJS, 182, 543
Abel, N. P., & Satyapal, S. 2008, ApJ, 678, 686
Chary, R., & Elbaz, D. 2001, ApJ, 556, 562
Chevalier, R. A., & Clegg, A. W. 1985, Nature, 317, 44
Crenshaw, D. M., Kraemer, S. B., & George, I. M. 2003, ARA&A, 41, 117
Dale, D. A., & Helou, G. 2002, ApJ, 576, 159
de Vaucouleurs, G. 1948, Annales d'Astrophysique, 11, 247
Debuhr, J., Quataert, E., & Ma, C.-P. 2012, MNRAS, 420, 2221
Diamond-Stanic, A. M., Rieke, G. H., & Rigby, J. R. 2009, ApJ, 698, 623
Di Matteo, T., Springel, V., & Hernquist, L. 2005, Nature, 433, 604
Elbaz, D., Dickinson, M., Hwang, H. S., et al. 2011, A&A, 533, A119
Fabian, A. C. 2012, arXiv:1204.4114
Farrah, D., Bernard-Salas, J., Spoon, H. W. W., et al. 2007, ApJ, 667, 149
Fazio, G. G., Hora, J. L., Allen, L. E., et al. 2004, ApJS, 154, 10
Gandhi, P., Horst, H., Smette, A., et al. 2009, A&A, 502, 457
Gilli, R., Vignali, C., Mignoli, M., et al. 2010, A&A, 519, A92
Granato, G. L., De Zotti, G., Silva, L., Bressan, A., & Danese, L. 2004, ApJ, 600, 580
Heckman, T. M., Armus, L., & Miley, G. K. 1990, ApJS, 74, 833
Heckman, T. M., Lehnert, M. D., & Armus, L. 1993, The Environment and Evolution of Galaxies, 188, 455
Heckman, T. M., Lehnert, M. D., Strickland, D. K., & Armus, L. 2000, ApJS, 129, 493
Heckman, T. M. 2002, Extragalactic Gas at Low Redshift, 254, 292
Heckman, T. M., Ptak, A., Hornschemeier, A., & Kauffmann, G. 2005, ApJ, 634, 161
Heckman, T. M., et al. 2011, ApJ, 730, 5
Hopkins, P. F., Cox, T. J., Dutta, S. N., et al. 2009, ApJS, 181, 135
Hopkins, P. F., Murray, N., Quataert, E., & Thompson, T. A. 2010, MNRAS, 401, L19
Hopkins, P. F., Quataert, E., & Murray, N. 2012, MNRAS, arXiv:1110.4638
Kennicutt, R. C., Jr. 1998, ApJ, 498, 541
Kormendy, J., Fisher, D. B., Cornell, M. E., & Bender, R. 2009, ApJS, 182, 216
Law, D. R., Steidel, C. C., Shapley, A. E., et al. 2012, ApJ, 745, 85
Lehnert, M. D., & Heckman, T. M. 1996, ApJ, 472, 546
Leitherer, C., Robert, C., & Drissen, L. 1992, ApJ, 401, 596
Leitherer, C., Schaerer, D., Goldader, J. D., et al. 1999, ApJS, 123, 3
Martin, C. L. 2005, ApJ, 621, 227
Martin, D. C., Fanson, J., Schiminovich, D., et al. 2005, ApJ, 619, L1
Meurer, G. R., Heckman, T. M., Lehnert, M. D., Leitherer, C., & Lowenthal, J. 1997, AJ, 114, 54
Moustakas, J., Zaritsky, D., Brown, M., et al. 2011, arXiv:1112.3300

Murray, N., Quataert, E., & Thompson, T. A. 2005, ApJ, 618, 569
Murray, N., Ménard, B., & Thompson, T. A. 2011, ApJ, 735, 66
Overzier, R. A., Heckman, T. M., Tremonti, C., et al. 2009, ApJ, 706, 203
Peng, C. Y., Ho, L. C., Impey, C. D., & Rix, H.-W. 2002, AJ, 124, 266
Peng, C. Y., Ho, L. C., Impey, C. D., & Rix, H.-W. 2010, AJ, 139, 2097
Polletta, M., Tajer, M., Maraschi, L., et al. 2007, ApJ, 663, 81
Robaina, A. R., Bell, E. F., van der Wel, A., et al. 2010, ApJ, 719, 844
Rodríguez Zaurín, J., Tadhunter, C. N., & González Delgado, R. M. 2008, MNRAS, 384, 875
Rieke, G. H., Alonso-Herrero, A., Weiner, B. J., et al. 2009, ApJ, 692, 556
Rubin, K. H. R., Weiner, B. J., Koo, D. C., Martin, C. L., Prochaska, J. X., Coil, A. L., & Newman, J. A. 2010, ApJ, 719, 1503
Rujopakarn, W., Rieke, G. H., Eisenstein, D. J., & Juneau, S. 2011, ApJ, 726, 93
Rujopakarn, W., Rieke, G. H., Weiner, B. J., et al. 2011, arXiv:1107.2921
Rupke, D. S., Veilleux, S., & Sanders, D. B. 2005, ApJS, 160, 115
Schlegel, D. J., Finkbeiner, D. P., & Davis, M. 1998, ApJ, 500, 525
Scoville, N. Z., Yun, M. S., & Bryant, P. M. 1997, ApJ, 484, 702
Sharma, M., & Nath, B. B. 2011, arXiv:1112.3447
Shapley, A. E., Steidel, C. C., Pettini, M., & Adelberger, K. L. 2003, ApJ, 588, 65
Shen, S., Mo, H. J., White, S. D. M., et al. 2003, MNRAS, 343, 978
Silk, J., & Rees, M. J. 1998, A&A, 331, L1
Steidel, C. C., Erb, D. K., Shapley, A. E., Pettini, M., Reddy, N., Bogosavljević, M., Rudie, G. C., & Rakic, O. 2010, ApJ, 717, 289
Thompson, T. A., Quataert, E., & Murray, N. 2005, ApJ, 630, 167
Tremonti, C. A., Moustakas, J., & Diamond-Stanic, A. M. 2007, ApJ, 663, L77
Trujillo, I., Conselice, C. J., Bundy, K., et al. 2007, MNRAS, 382, 109
van Dokkum, P. G., et al. 2008, ApJ, 677, L5
Veilleux, S., Cecil, G., & Bland-Hawthorn, J. 2005, ARA&A, 43, 769
Veilleux, S., Kim, D.-C., Peng, C. Y., et al. 2006, ApJ, 643, 707
Weiner, B. J., et al. 2009, ApJ, 692, 187
Werner, M. W., Roellig, T. L., Low, F. J., et al. 2004, ApJS, 154, 1
Wright, E. L., Eisenhardt, P. R. M., Mainzer, A. K., et al. 2010, AJ, 140, 1868
Wuyts, S., Cox, T. J., Hayward, C. C., et al. 2010, ApJ, 722, 1666
Wuyts, S., Förster Schreiber, N. M., van der Wel, A., et al. 2011, ApJ, 742, 96